High-Speed, Random-Access Fluorescence Microscopy: I. High-Resolution Optical Recording with Voltage-Sensitive Dyes and Ion Indicators

A. Bullen,*# S. S. Patel,* and P. Saggau*
*Division of Neuroscience, Baylor College of Medicine, Houston, Texas 77030, and #Department of Physiology, University of Pennsylvania School of Medicine, Philadelphia, Pennsylvania 19104

ABSTRACT The design and implementation of a high-speed, random-access, laser-scanning fluorescence microscope configured to record fast physiological signals from small neuronal structures with high spatiotemporal resolution is presented. The laser-scanning capability of this nonimaging microscope is provided by two orthogonal acousto-optic deflectors under computer control. Each scanning point can be randomly accessed and has a positioning time of 3–5 μs. Sampling time is also computer-controlled and can be varied to maximize the signal-to-noise ratio. Acquisition rates up to 200k samples/s at 16-bit digitizing resolution are possible. The spatial resolution of this instrument is determined by the minimal spot size at the level of the preparation (i.e., 2–7 μm). Scanning points are selected interactively from a reference image collected with differential interference contrast optics and a video camera. Frame rates up to 5 kHz are easily attainable. Intrinsic variations in laser light intensity and scanning spot brightness are overcome by an on-line signal-processing scheme. Representative records obtained with this instrument by using voltage-sensitive dyes and calcium indicators demonstrate the ability to make fast, high-fidelity measurements of membrane potential and intracellular calcium at high spatial resolution (2 μm) without any temporal averaging.

INTRODUCTION

Optical indicators of membrane potential or intracellular ion concentration have become an important tool for many types of biological investigation. Experiments with these indicators have employed a variety of detection schemes. In many cases, scientific-grade video cameras or confocal microscopes are used to obtain a series of high-resolution images that contain physiological information. However, these methods cannot be universally applied because they have limited temporal bandwidth and commonly employ only modest digitizing resolution. This is particularly evident in studies using voltage-sensitive dyes (VSDs), in which signal sizes are small and high temporal resolution is required. Instead, signals from these probes are commonly measured with photodiode arrays (PDAs). These detectors provide less spatial resolution but a larger temporal bandwidth and better signal quality than other imaging detectors. This report documents an alternative approach to measuring these signals. Specifically, a new nonimaging microscope that utilizes a nontraditional scanning approach is proposed. This system has been optimized to make high-fidelity recordings from VSDs and ion indicators while achieving very high spatiotemporal resolution.

Fast VSDs are potentiometric membrane probes that are commonly used to investigate problems and/or preparations where the use of multielectrode approaches would be difficult or impossible (for reviews see Cohen and Salzberg, 1978; and Loew, 1993). Furthermore, these dyes possess several properties that make them superior to classical electrophysiological techniques for many types of experiments. In particular, they are noninvasive and allow long-term measurements with high spatial and temporal resolution. However, the instrumental requirements necessary to record synaptic and action potentials from small neuronal structures with VSDs are rigorous. In particular, the system bandwidth necessary to adequately capture these signals is quite high (>1 kHz). Moreover, the structures of interest in mammalian central nervous system neurons are relatively small (1–10 μm); consequently, signal strength is often weak. Furthermore, because the signal sizes generated by most VSDs are small, signal-to-noise considerations must be optimized and high-resolution digitization is required. In contrast, the signals from calcium indicators are larger and the temporal bandwidth required is less. Hence the instrumental requirements for recording these signals are less exacting.

To date, multisite optical recording with VSDs has been applied to neural preparations by employing conventional microscopic techniques (Salzberg et al., 1977; for reviews see: Cohen et al., 1989; Grinvald, 1985; Lieke et al., 1989; Salzberg, 1983, 1989; Ebner and Chen, 1995). However, the small signal size inherent in many VSDs has required the use of extremely stable light sources, and in many cases, signal-averaging techniques were also necessary. Such techniques were necessary to achieve a sufficient signal-to-noise ratio, eliminated nonstationary events from consideration. Moreover, this problem has precluded the use of lasers, which are inherently noisy light sources (Cohen and Lesher, 1986). Variations in laser light intensity are on the order of

Received for publication 10 December 1996 and in final form 17 April 1997.

Address reprint requests to Dr. Peter Saggau, Division of Neuroscience, Baylor College of Medicine, One Baylor Plaza, Houston, TX 77030. Tel.: 713-798-5082; Fax: 713-798-3946; E-mail: psaggau@bcm.tmc.edu.

0006-3495/97/07/477/15 $2.00

1–5%, which is about equal to or greater than the average signal size obtained from most VSDs. Because lasers are the light source of choice for scanning systems, this approach is not commonly employed in VSDs studies. However, if this limitation could be overcome, laser-based scanning systems would offer several distinct advantages over comparable nonscanning systems. Such advantages include less light scattering and a reduction in the total illumination seen by the preparation. The reduction in light scattering arises from the nature of intermittent point illumination (versus full field illumination), where scattering from neighboring points is absent. The reduction in total illumination is advantageous because of decreased photodynamic damage and less dye bleaching, both of which facilitate longer recording episodes. In some circumstances an increase in spatial resolution can also be achieved with scanning systems. Furthermore, instruments with point illumination can easily be extended to become confocal systems with a corresponding increase in spatial resolution.

RANDOM-ACCESS FLUORESCENCE MICROSCOPY

There are several commonly used variations of quantitative fluorescence microscopy that could be adapted for recording from fluorescent indicators (Fig. 1). These variations can be grouped into scanning and nonscanning applications. In nonscanning approaches, spatial resolution is achieved with multielement detectors such as photodiode arrays and imaging cameras. In contrast, scanning methods typically use a spatially nonresolving detector and build up an image by sequentially visiting each point. The resolution of this image depends on the size of the scanning spot and the accuracy with which it can be positioned.

For any of these approaches to be useful in physiological studies, several factors must be considered: temporal bandwidth, sensitivity, and spatial resolution. Cost and ease of use are additional factors to be considered. The relative merits of each approach for physiological studies are outlined in Table 1. Of these methods, line scanning and photometry typically provide the largest temporal bandwidth, but little or no spatial information. In contrast, imaging detectors (e.g., cooled CCD camera) can exhibit high sensitivity and produce high spatial resolution images, but commonly possess very limited temporal bandwidth and are expensive. Confocal microscopes typically operate in a raster scanning mode and achieve superior spatial resolution by rejection of out-of-focus light (reviewed in Pawley, 1995). However, in this mode, temporal resolution is poor and high illumination intensities are required. Therefore, these instruments have limited usefulness for the acquisition of fast physiological signals. Although some modern confocal microscopes can operate in a line-scanning mode and temporal resolution is somewhat increased by using this regime (i.e., up to 200 Hz), preparations must be correctly aligned to enable use of this feature.

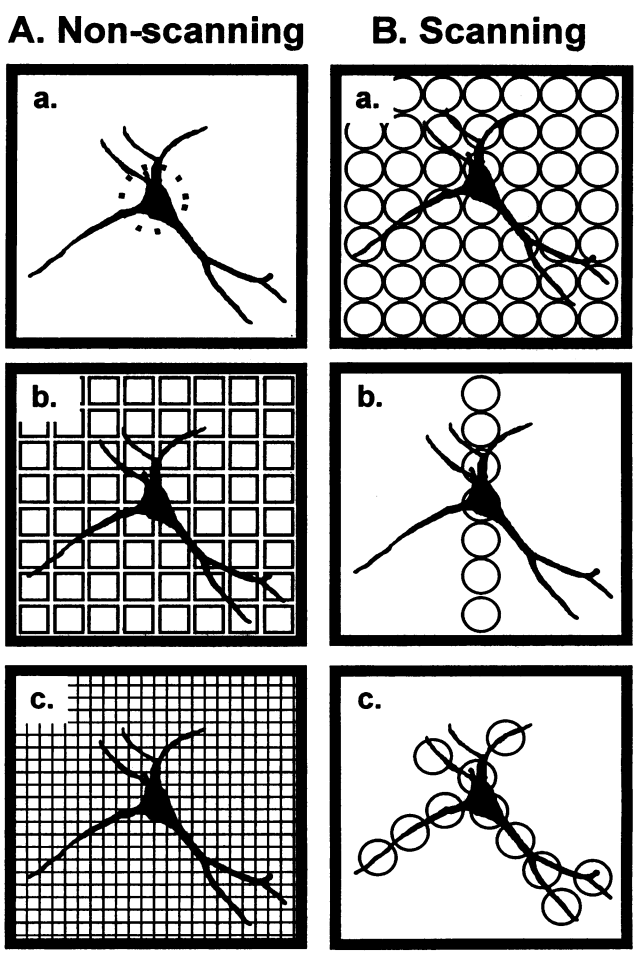

FIGURE 1 Fluorescence microscopy. Schematic representation of selected types of fluorescence microscopy commonly used in physiological investigations. (*A*) Nonscanning microscopy. *a*: Photometry. *b*: Photodiode array. *c*: Imaging detector (e.g., cooled CCD camera). (*B*) Scanning microscopy. *a*: Raster scanning (e.g., confocal microscope). *b*: Line scanning. *c*: Random-access scanning. Note that scanning spot and pixel sizes are not drawn to scale and other variations are possible.

Previously, silicon PDAs have been used to record fast physiological signals, especially those arising from VSDs (reviewed in Wu and Cohen, 1993). These detectors possess a high quantum efficiency (0.9), particularly at the long wavelengths emitted by VSDs, and thus can yield a higher signal-to-noise ratio than equivalent devices with lower quantum efficiencies (Cohen and Lesher, 1986). PDAs typically include between 10 and 24 photodiode elements per dimension. However, element size and position in these arrays are always fixed; thus, in many cases only modest spatial resolution can be achieved. Furthermore, the electronics associated with these arrays are complicated and not easily varied to accommodate different temporal bandwidths and/or sensitivities.

An alternative approach to measuring VSD signals with silicon PDAs is a laser-based random-access scanning system. Such an approach has a number of advantages when compared to existing PDA systems. For instance, random-

TABLE 1 Characteristics of common methods in fluorescence microscopy

	Nonscanning			Scanning		
	Single detector (photometry)	Photodiode array	Imaging detector	Raster scanning	Line scanning	Random-access scanning
Temporal resolution	High	Intermediate	Poor	Poor	High	High
Spatial resolution	None	Intermediate	High	High	One-dimensional	High
Compatible with VSD signals	Yes	Yes	No	No	Yes	Yes

access scanning can provide higher spatial resolution, greater flexibility in point selection, and a reduction in the total illumination required. Additionally, there is less total light scattering from a laser point source (versus full-field illumination), and therefore unspecific fluorescence is reduced. Moreover, the detector electronics for this scanning mode can be very simple and easy to manipulate for various temporal bandwidths and/or sensitivities. After considering the merits of the preceding approaches to fluorescence microscopy, we have designed and built a novel random-access scanning system optimized for the acquisition of fast physiological signals.

SCANNING MECHANISMS

To obtain a fast scanning point source that can be randomly addressed, a number of beam scanning methods could be utilized. These methods can be loosely grouped into two categories: reflection scanning and diffraction scanning (for review see Wilson and Sheppard, 1984). Reflection scanners include servo-controlled galvanometric mirrors, resonant galvanometers, and rotating polygons that are used to deflect a laser beam. Most of the commercially available scanning microscopes are based on this type of scanner. An obvious advantage of reflection scanning is that it is wavelength independent. However, this is balanced by its mechanical nature, which restricts high scanning rates, makes nonraster scanning applications difficult, and can generate mechanical noise.

Diffractive scanning methods commonly employ acousto-optic devices. These devices utilize the diffraction effect induced by optical gratings to achieve laser beam deflection (for a review see Xu and Stroud, 1992). An acousto-optic scanner utilizes sound waves to produce periodic alterations in the refractive index of an optically transparent medium (e.g., $PbMoO_4$ or TeO_2). These alterations in refractive index act like a diffraction gradient. In solid-state acousto-optical (AO) devices, the grating constant is variable and can be controlled by the frequency of a planar sound wave traveling through the AO medium (for a review see Milton et al., 1983). Rapid manipulation of the acoustic frequency allows these devices to be used as very fast one-dimensional deflectors. This is an important advantage of AO scanning, because it allows individual points to be directly addressed and therefore provides a fast random-access scanning capability. A two-dimensional scanner is formed by two such devices arranged orthogonally.

In this report we outline the design and implementation of a high-speed, random-access, laser-scanning fluorescence microscope constructed from acousto-optical devices. An earlier version of this microscope previously developed in our laboratory (Saggau et al., 1990) utilized a simple raster-scanning scheme to record population signals generated by VSDs in brain slice preparations (Saggau, 1994; Sutor et al., 1994). This system possessed relatively poor spatial resolution and covered only a modest scanning area. Typically, signal averaging was employed to achieve the required signal-to-noise ratio. Recently we have developed a more advanced instrument based on a similar scanning mechanism, but designed to record nonstationary signals with higher spatiotemporal resolution over a larger scanning area. This instrument implements a random-access scanning scheme designed to record from optical indicators under conditions where the signal size is small and high spatiotemporal resolution is required. Using the first implementation of this methodology combined with patch-clamp techniques, we have investigated voltage and ion concentration transients on the subcellular level in cultured hippocampal neurons. In particular, we have shown that this instrument is useful for making measurements of membrane potential and intracellular ion concentration during evoked and synaptic events with high spatial and temporal resolution.

Preliminary reports of this work were previously published in abstract form (Bullen and Saggau, 1994, 1995).

MATERIALS AND METHODS

AO deflection

AO devices can operate in two different modes: Debye-Sears or Ramath-Nath mode and the Bragg mode (reviewed in Milton et al., 1983). Operation in the Bragg mode is most common and was employed here. Under this condition, most of the laser light incident on the AO media will be diffracted into a first-order spot that is separated from the zero-order spot by the "deflection angle."

The design considerations for a scanning system incorporating AO devices operating in this mode are fundamentally different from those of traditional microscopes. In particular, the nature and extent of deflection with acousto-optic devices are governed by a unique set of physical principles. These principles dictate many of the operational parameters of this microscope. Such parameters include the size of the deflection angle, random-access time, scanning spot size, and the resolution generated by these devices. Many of these parameters are interrelated, and several trade-offs were required during the implementation of this approach. Some of these interrelationships are briefly documented below.

The size of the deflection angle and hence the area that can be scanned

by orthogonal deflectors is defined by

$$\Theta_\tau = \lambda \Delta\phi / v_a \quad (1)$$

where Θ_τ is the deflection angle, λ is the wavelength of light being used, $\Delta\phi$ is the bandwidth of the acoustic frequency, and v_a is the velocity of sound in the optical medium. Thus deflection angle is proportional to the acoustic bandwidth and inversely proportional to the acoustic velocity; therefore, generation of relatively large scan angles requires that deflectors operate with a large acoustic bandwidth (i.e., 40 MHz) and/or a low acoustic velocity (i.e., 620 m/s for TeO_2).

Scanning spot size (S) is dictated by

$$S \propto 1/D \quad (2)$$

where D is the beam diameter or aperture size of the deflector (whichever is smaller). An important implication of this relationship is that diffraction of a wider beam typically results in a smaller scanning spot. However, the wider an aperture or beam, the longer it takes for a new sound wave to transverse its width. This in turn limits the random-access time of the deflector and, therefore, the maximum rate at which the laser beam can be positioned. Thus there is a trade-off between spot size and absolute scanning rate.

Deflector resolution is defined as the number of independent spots that can be generated across the deflection angle. There is also a close relationship between the resolution of an AO deflector (AOD) and aperture or beam size. Two equations describe this relationship:

$$N = \tau \Delta\phi \quad (3)$$

and

$$\tau = D/v_a \quad (4)$$

where N is the number resolvable points and v_a is the acoustic velocity. The aperture time (τ) is sometimes termed the "time-bandwidth product" and represents the time the acoustic wave takes to fill the aperture. These equations indicate that the transit time of the acoustic waves across the laser beam and the transducer bandwidth both limit resolution. The time required for the acoustic wave to fill the aperture is a function of the velocity of sound in the optical medium and the width of the laser beam. Consequently, an increased resolution can be achieved by increased acoustic bandwidth, increased beam diameter, or decreased acoustic velocity.

To summarize, a deflector that operates over a large scan angle with high resolution should posses a large acoustic bandwidth and/or a low acoustic velocity. Correspondingly, deflectors required to produce a relatively small spot size should have a large aperture. However, this aperture should not be so large as to limit the random-access time of the deflector. Hence, in designing a scanning system based on AO deflection, a compromise must be made between spot size, resolution, scan angle, and scanning speed. In many instances, the criteria for establishing these parameters will depend on the prevailing experimental objectives.

AO deflection can also be achieved with acousto-optic modulators (AOMs). These devices are essentially similar to AODs, but are primarily designed to modulate the intensity of light by manipulating the amplitude of the sound wave. However, under the correct conditions, they are also able to act as deflectors. The main advantage of AOMs over AODs is that they possess higher acoustic velocities and, therefore, shorter random-access times and higher maximum scanning rates. Unfortunately, this fast access time is balanced by decreased resolution and smaller scan angles. Both AODs and AOMs are used here, depending on the instrumental requirements (see below).

Random-access laser scanning microscope

The random-access laser-scanning microscope system described here is based on an AO deflection mechanism and consists of five major components: a laser, a scanning unit, a microscope, a detection unit, and a dedicated computer. The complete system was constructed on a vibration-isolated table (Xl/KNS series; Newport) to avoid external mechanical noise. A detailed scheme of the laser and associated scanning unit is shown in Fig. 2.

Laser

A continuous-wave argon ion laser (164-46; SpectraPhysics) was employed as a monochromatic point source. Both primary lines (e.g., 488 and 514 nm) of this laser were tested for their suitability for optical recording. The light stabilization mode available in this laser was not used, as it lacked sufficient bandwidth and failed to enhance the noise performance of the overall system.

A beam expander with spatial filter was incorporated in the optical path before the first deflector. The beam expander serves to better fill the entry aperture of the first deflector, thereby decreasing final spot size, while the spatial filter increases the quality of this spot. This device was constructed from a 2.5× telescope (f40 and f100 lenses) and a 30-μm pinhole. A further 2-mm aperture was positioned immediately before the first deflector to adjust the final beam shape and size, and to reduce extraneous scattered light entering the deflector.

Scanning unit

The scanning unit is based on a high-precision optical bench (MicroBench; Spindler and Hoyer) and contains two orthogonal acousto-optical deflectors (Isomet; see Table 2) operated in the Bragg mode (for a review, see Xu and Stroud, 1992). Interchangeable sets of these devices were incorporated to generate either high temporal resolution scanning (AOMs; Isomet 1205C) or high spatial resolution scanning (AODs; Isomet LS55V). The performance characteristics of the deflector combinations used in this project are compared in Table 2.

The actual position of the laser beam is governed by two control voltages provided by a computer-controlled two-channel digital-to-analog (D/A) converter (PCIP-AWFG; Keithley-Metrabyte). The precision of spot placement is dictated by the 12-bit resolution of these D/A converters (i.e., 4096 independent locations per dimension). These control voltages are converted by two frequency modulators (D322B, Isomet) to provide the input frequencies to each AOD. A scheme showing the laser beam profile and its transformation at each stage is depicted in Fig. 2 *B*. This figure documents how a single scanning spot is isolated from the complex diffraction pattern by passing the first-order diffraction maxima and obstructing all others. The zero-order and second- or higher-order diffraction maxima were obstructed by two slits positioned by a pair of adjustable micrometers.

A series of relay telescopes were employed to expand the initial scanning pattern after it exited the final deflector and to project it to the back focal plane of the objective. These telescopes were composed of achromatic lenses (06 series; Spindler and Hoyer) with magnifications matched to the corresponding deflector combination (see Table 2).

Microscope

The microscope is based on an optical-bench-based inverted-type epifluorescence system (MicroBench) fitted with an objective lens suited for scanning application (Fluar, 100×, N.A. 1.3; Zeiss). A scheme detailing the important optical components in this system is depicted in Fig. 3.

This microscope was specially designed to perform optical measurements and patch-clamp recordings simultaneously. For this purpose, it is equipped with a commercial illuminator (Zeiss) and a custom stage able to translate the preparation relative to the objective (not shown). The differential interference contrast (DIC) optics included with this illuminator are paired with a matched prism and polarizer, both of which are situated in a custom housing beneath the objective. Typically, the polarizer was removed during optical recording.

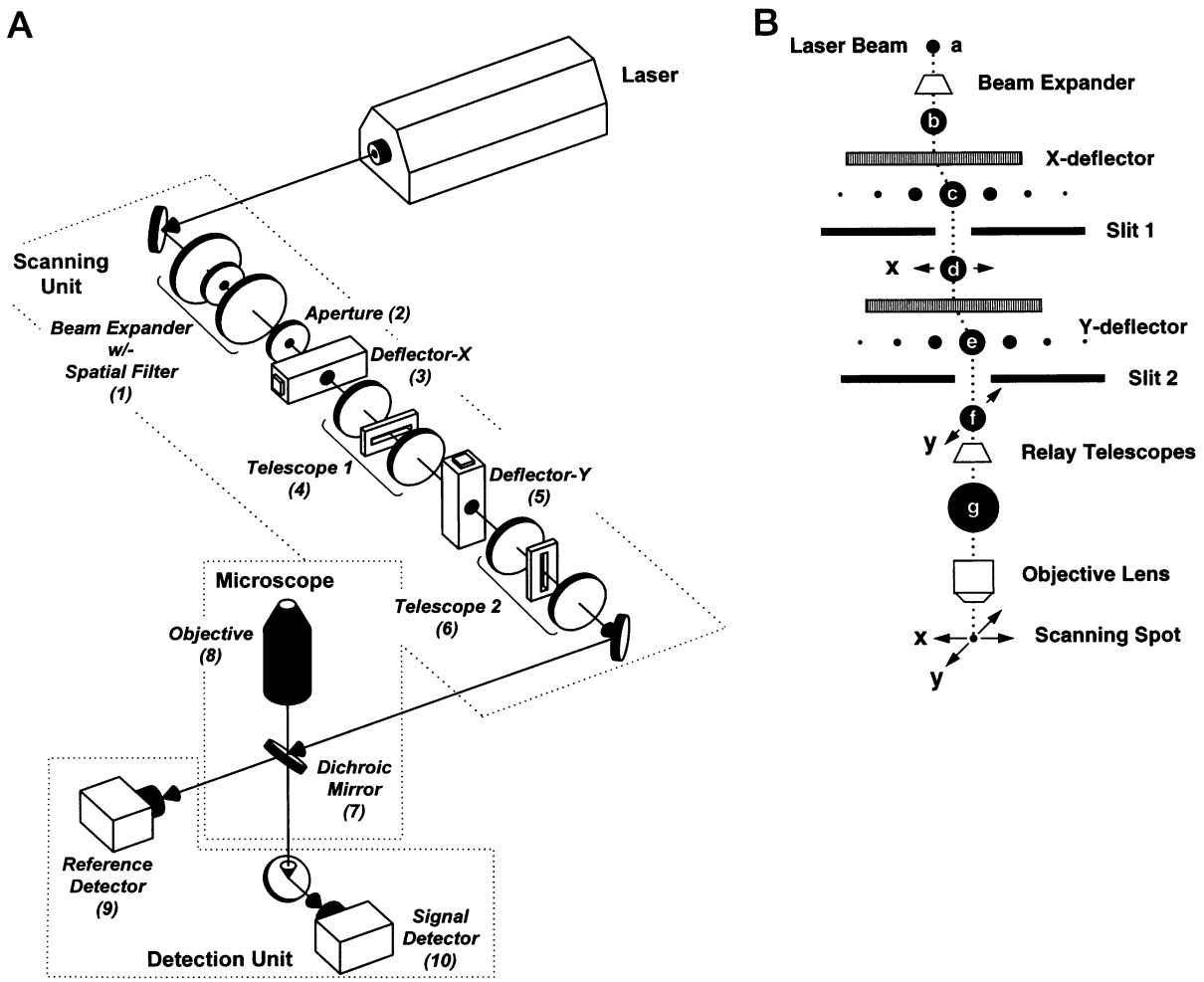

FIGURE 2 Schematic representation of a high-speed random-access laser scanning microscope. (*A*) This instrument is composed of three main parts: i) Laser: a continuous-wave argon ion laser (λ = 514 nm). ii) Scanning unit, including beam expander (2.5× telescope and 30-μm pinhole) (*1*); aperture (2 mm) (*2*); X-deflector (*3*); telescope 1, including slit 1 (*4*); Y-deflector (*5*); and telescope 2, including slit 2 (*6*). iii) Microscope unit, including dichroic mirror (*7*), objective (*8*), and other transillumination and DIC optics not shown. iv) Detection unit, including reference detector (*9*) and signal detector (*10*). Three relay telescopes are also omitted for clarity. (*B*) Schematic representation of the laser beam at different stages of scanning. *a*: Initial laser beam. *b*: Expanded and filtered laser beam. *c*: Diffracted beam, *x* dimension. *d*: First-order diffraction spot, *x* dimension. *e*: Diffracted beam, *y* dimension. *f*: First-order diffraction spot, *y* dimension. *g*: Expanded scanning spot. *h*: Focused scanning pattern at the level of the preparation. Note: the size of each diffraction spot is approximately proportional to its intensity. The largest spots represent the first-order diffraction maxima.

Detection unit

The detection unit includes two types of detectors: 1) photodiodes for recording fluorescence and sampling excitation light, and 2) a video camera for visualizing the preparation. A switchable mirror was used to direct emitted fluorescence or transillumination light to its respective detector.

Detectors for optical recording

This element consists of two independent photodiodes (1336K2G; Hamamatsu) operated in the photovoltaic mode. One photodiode serves as the primary signal detector, while a second photodiode is used as a reference detector. Emission light collected by the objective lens is translated to its respective detector by relay optics and focused to a small spot (<1 mm^2) on the signal diode (active area 1.2 mm^2). In contrast, the reference detector measures a small fraction of the excitation light that passes through the dichroic mirror, at a point equivalent to the back focal plane of the objective. Before reaching this point, the light is further attenuated and a diffuser is used to eliminate the scanning pattern. Each photodiode included a low noise, op-amp-based (OPA606) transimpedance circuit. Several variations of this custom-built circuit were employed, depending on signal strength, response time, and required bandwidth. For the purpose of ratio measurements, both detector signals were simultaneously sampled, multiplexed, and digitized by a high-resolution (16-bit) and high-speed (1 MHz) A/D converter (Fast-16; ANALOGIC). The high temporal precision of the simultaneous sample and hold circuit was required to ensure correct ratio formation. Only a slight temporal offset in these ratios resulted in a dramatically decreased signal-to-noise ratio. The frequency responses of the preamplifier circuits for both signal and reference detectors were carefully matched to ensure against aliasing and phase shifts.

Detector for visualization

A commercial tube camera (WV-1550; Panasonic) was used to acquire a reference DIC image from the preparation. The output signal of the video

TABLE 2 Performance characteristics of acousto-optical devices

	Low-resolution AOM* (Isomet 1205C)	High-resolution AOD# (Isomet LS55V)	Dependent on AO property	Functional consequences
Spot size§	7 μm	2 μm	System magnification and scan angle	Spatial resolution and signal-to-noise
Resolution per dimension¶	15	65	Time/bandwidth product‖	Spatial resolution
Scan angle and scan area**	56 mrad. or 100 μm per dimension @ 10× mag.	80 mrad or 130 μm per dimension @ 2× mag.	Deflector bandwidth	Scanning field size
Diffraction efficiency##,§§	40–80% Dependent on scan angle	60% Independent of scan angle	Optical medium¶¶	Uniformity of illumination and signal-to-noise
Maximum scan rate	200k points per second	100k points per second	Acoustic velocity and aperture time	Number of points and temporal resolution

* AOM, acoustooptic modulator.
\# AOD, acoustooptic deflector.
§ Spot size with 100× objective.
¶ Number of resolvable spots per dimension as determined by the Rayleigh criteria.
‖ Time/bandwidth product is an indicator of the useful resolution of an AO devices.
** After magnification by the scanning system and 100× objective.
Diffraction efficiency describes the amount of laser light concentrated in the first-order diffraction spot.
§§ Diffraction efficiency as determined with linearly polarized light.
¶¶ TeO_2 or Pb MoO_4.

camera was digitized by a real-time frame grabber with VGA overlay capability (Ecomedia). This system could be operated either in "live" mode to visualize the preparation during cell selection or in "grab" mode to store images. An emission filter (Schott, OG530) positioned directly in front of this camera excluded stray excitation light.

Alignment

Registration of the scanning grid and the accompanying video image is achieved by a simple alignment procedure. In this process, a test preparation of uniformly fluorescent dye is used to generate a video image of the scanning pattern. This image is then interactively adjusted to coincide with the computer's internal representation of the scanning grid. This alignment procedure was confirmed by periodic tests conducted on cellular structures selected for optical recording.

Computer

Both the scanner unit and the detector unit are controlled by a single dedicated computer (AT-486, Windows 95). Three processes were run concurrently on this computer: the scanning unit is provided with the spatiotemporal beam deflection pattern, the ratio algorithms are computed, and the physiological signals are topographically displayed on the reference image. This was made possible by providing both the D/A converter system used by the scanner and the D/A converter system used by the detector unit with private memory. This feature enabled this instrument to avoid the speed limitations inherent in the computer's ISA bus.

Software

The nature of the experimental approach proposed here requires a versatile computer interface that allows the investigator to focus on the experiment rather than on the recording system. This was achieved by employing a Windows-based graphical user interface that shielded the operator from much of the instrumental complexity. For example, each scanning site is chosen by point-and-click selection within a calibrated display window. These recording sites are subsequently registered with the stored image of the preparation, and control voltages for each deflector are automatically calculated by system software. In a similar manner, raw signals that were captured during an experiment are processed into useful optical signals by using various averaging and digital filtering routines that are built directly into the software. These signals are then topographically displayed on the reference image to allow for further interactive data handling.

Noise reduction

The amplitude fluctuations of available lasers with suitable parameters for optical recording, such as output power, wavelength, etc., require noise reduction procedures to be employed. This could be achieved by either feedback control or by computation. Feedback control aims to actively improve the amplitude stability, whereas correction by computational procedures can take several forms (i.e., subtraction or ratio formation). Here we have chosen to perform ratio measurements of emission light coming from the preparation versus excitation light going to the preparation. The theoretical foundation behind this decision arises from the following relationships. In general, fluorescence (F) is proportional to the product of illumination intensity (I) and the total quantum efficiency (Q, emitted photons per absorbed photon):

$$F \propto Q \times I \tag{5}$$

However, there are significant fluctuations (ΔI) in illumination intensity (I) from laser sources, and these fluctuations are reflected in emitted fluorescence:

$$F + \Delta F \propto Q \times (I + \Delta I) \tag{6}$$

The signal of interest is derived from changes in total quantum efficiency (ΔQ) that arise from changes in membrane potential or intracellular ion concentration. Thus Eq. 6 now becomes

$$F + \Delta F \propto (Q + \Delta Q)(I + \Delta I) \tag{7}$$

Although ΔQ and ΔI cause changes in fluorescence (F), only ΔQ contains the signal of interest. However, the contribution of ΔI can be removed by forming the ratio

$$\frac{F + \Delta F}{I + \Delta I} = Q + \Delta Q \tag{8}$$

Thus the signal of interest is retained and the contamination due to the laser beam intensity fluctuations is eliminated. The relative change in the emit-

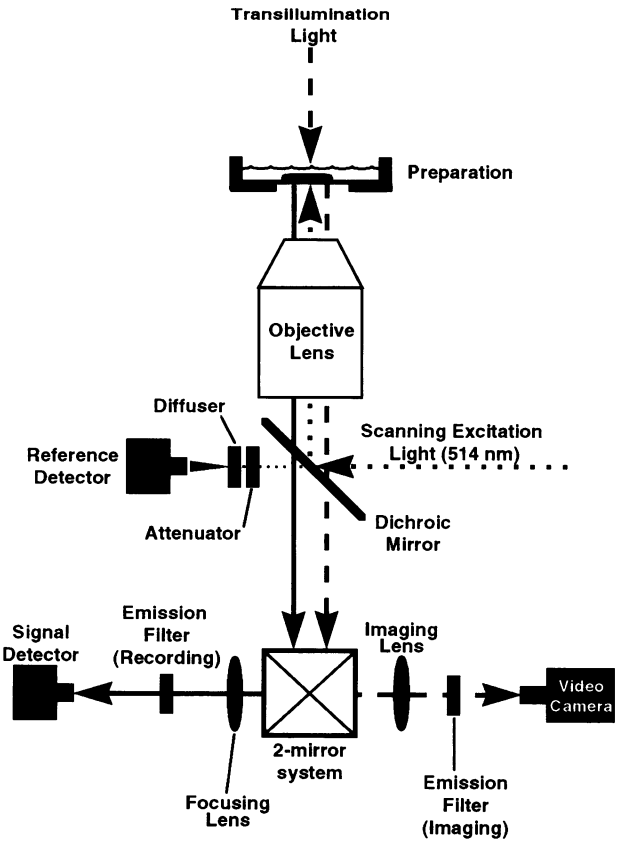

FIGURE 3 Epifluorescence microscope. Epifluorescence configuration for the high-speed random-access, laser-scanning microscope. Dichroic mirror: DCLP525 (Chroma Technology). Objective lens: Fluar 100× (Zeiss). Emission filters were RG590 (Schott) and OG550 (Schott) for voltage-sensitive dyes and calcium orange, respectively. An attenuator situated immediately in front of the reference detector is used to vary the amount of light incident on this detector. A diffuser, also situated at this point, was used to remove any variations in intensity arising from the focused scanning pattern. Additional transillumination and DIC optics omitted for clarity.

ted fluorescence can then be computed by

$$\frac{Q + \Delta Q}{Q} = 1 + \frac{\Delta Q}{Q} \tag{9}$$

where $\Delta Q/Q$ reflects the relative change in fluorescence after normalizing by its mean.

A practical implementation of this scheme is shown in Fig. 4. This approach requires that two quantities be measured concurrently: excitation light and emitted fluorescence. In this figure, excitation light is sampled by the reference detector and is designated *R*. Likewise, emitted fluorescence, which is the product of signal and variations in laser intensity, is sampled at the signal detector and is designated *S*. The true fluorescence signal (*F*) arising from the preparation is derived by dividing *S* by *R*. Computationally, the value *F* is obtained on a point-by-point basis from ratios of the corresponding signal and reference values. These quantities are simultaneously sampled and digitized at 16-bit resolution. Time-varying signals of *F* are calculated by normalizing each point relative to the mean of *F* for the whole record (i.e., $\Delta F/F$). To remain consistent with existing literature, the final filtered signal in this scheme is designated $\Delta F/F$. This value should not be confused with *F* terms given earlier (Eqs. 5–8), which refer to a pure fluorescence parameter.

RESULTS

Signal processing and noise reduction

A noise reduction scheme was definitely required to remove variations in laser intensity that contaminated fluorescent signals measured with this instrument. In particular, the signal-to-noise ratio achievable with VSD in the absence of noise reduction procedures or averaging was only 1–3 for a 100-mV action potential. However, incorporation of the ratiometric approach depicted in Fig. 4 improved this value significantly. The success of this method is apparent in the final panel of Fig. 4 (also see Representative Records). Comparative tests showed this procedure to be superior to correction by subtractive strategies, which required that the magnitude of each signal source (signal and reference) be exactly matched in size.

The overall stability of this system results in a good signal-to-noise ratio when compared with other studies that have used this indicator (di-8-butyl-amino-naphtyl-ethyl-ene-pyridinium-propyl-sulfonate; Cummings et al., 1992; Rohr and Salzberg, 1994a,b), or others that have employed laser sources to make VSD measurements (Grinvald and Farber, 1981). Typically, the signal-to-noise ratio achieved from spontaneous or evoked action potentials (i.e., ~100 mV) ranged between 20 and 30. In many instances, this variability could be attributed to slight differences in dye staining conditions or the relative amount of background fluorescence from nonneuronal structures in the recording chamber (e.g., glia). The signal-to-noise ratio for smaller postsynaptic potentials was less consistent. In the best cases, a signal-to-noise ratio of 5 could be recorded for these signals, but this was still achieved without any averaging.

Variations in signal strength (i.e., fluorescence) between scanning points or bleaching across trials were automatically corrected by considering only the relative change in fluorescence intensity (i.e., $\Delta F/F$). However, the high light intensities used here sometimes resulted in a small amount of dye bleaching within a single experimental sweep. When required, this bleaching was corrected in one of two ways. In traces where the signal of interest represented a small relative deflection compared to the whole record, a single exponential line was fitted to the overall signal and then subtracted. An example of this type of correction and a representative fit are also documented in Fig. 4. In other cases, an equivalent bleaching trace, without stimulus, was recorded and later subtracted from the original record.

The quality of these optical signals is due mainly to the applied ratio techniques and allows optical multisite recordings without the need to employ spatial and/or temporal averaging. However, at submaximum scanning rates, there is also a provision within this system to oversample or integrate each point as a means of improving the signal-to-noise ratio. The extent of oversampling is controlled in software, and the relative amount of noise reduction is roughly proportional to the square root of the number of

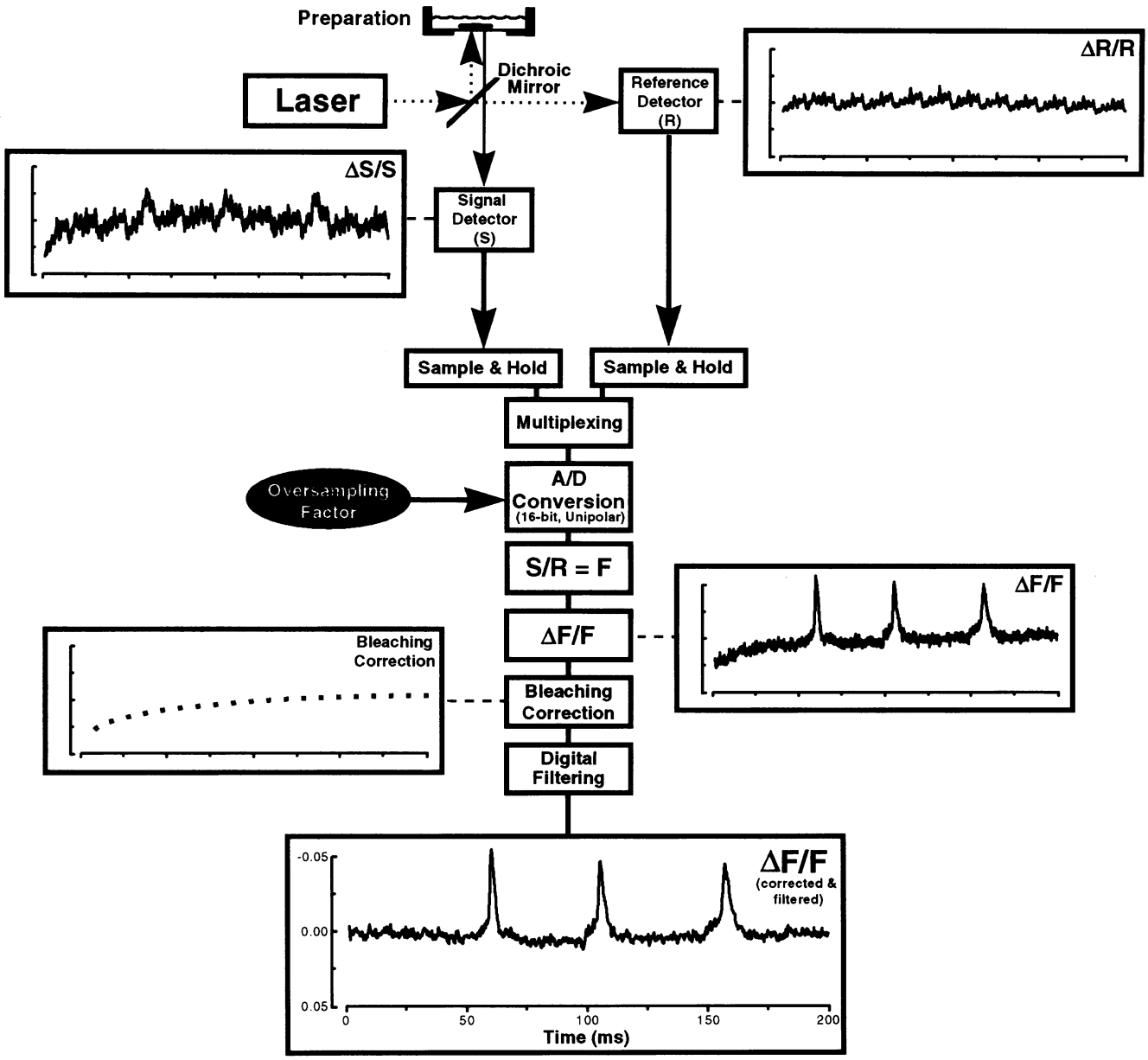

FIGURE 4 Signal-processing scheme. Schematic representation of the online signal-processing scheme that is employed to remove intrinsic variations in laser intensity. Representative records of the time-varying records before ratio formation (signal, $\Delta S/S$; reference, $\Delta R/R$) and the corrected signals ($\Delta F/F$) at various stages of processing are shown. The underlying signal was derived from a single scanning spot on the soma of a cultured hippocampal neuron. Three action potentials were elicited by current injection (200 pA) through a patch pipette (4 MΩ) on the soma. Both optical signals were sampled at 6 kHz and later smoothed using a low-pass digital filter (1.5 kHz; Hamming window). A bleaching correction was achieved by fitting (and subtracting) an exponential curve (shown in *box*) to $\Delta F/F$. The oversampling factor is a noise reduction feature that indicates the number of samples made each time the laser beam visits a selected point. Multiple samples are averaged to give the mean fluorescence for that point.

extra samples made, as would be predicted from theoretical considerations.

Spatiotemporal resolution

The size of the scanning spots and total scanning area in this system are the products of two factors: deflector characteristics and system magnification. The exact number of spots per dimension and relative scan range are properties of the deflectors used. Typical values for the deflector combinations are given in Table 2. System magnification is the product of the magnification of the relay telescopes in the optical bench and the magnification of the objective lens. Two objective lenses have been tested: 40× and 100×. In practice, the latter gave the best results because of its high numerical aperture (1.3, Fluar; Zeiss). The magnitude of intermediate magnification provided by these relay telescopes was dictated by the type of AO device used. Typi-

cally, the intermediate magnification was adjusted so that the scanning pattern maximally filled the aperture of the objective. The values used for each deflector combination are documented in Table 2. The spatial resolution of the system was determined by the smallest spot size at the level of the preparation. In practice, the best spatial resolution achieved with this instrument was 2 μm, and this allowed subcellular resolution in recordings from small mammalian central nervous system neurons in culture.

The current version of the laser scanning system is capable of recording up to 100 spots per frame. This value is currently limited by software constraints; much higher numbers are possible. However, in contrast to raster scanning, each spot is interactively selected; consequently, a typical experimental sweep usually included less than 10 points of interest.

The temporal resolution achieved with the current system was continuously variable down to microsecond values. However, in practice, it was varied to match the experimental circumstances and detector bandwidth. The minimum frame rate used here was 2 kHz. This value is easily sufficient to monitor fast events such as synaptic potentials and action potentials. Typically, higher values were used (i.e., 5 kHz), and the resulting signals were then digitally filtered (i.e., 1–2 kHz) to further improve signal quality.

Representative records

Examples of the signal quality generated in experiments with this system are documented in Figs. 5, 6, and 7. All records represent single sweep measurements and are processed in the manner described in Fig. 4. No averaging techniques were employed.

Membrane potential signals were acquired using the voltage-sensitive dye di-8-ANEPPS (Molecular Probes), which was applied by bath application. The fidelity of recordings made with this probe can be assessed by comparing the

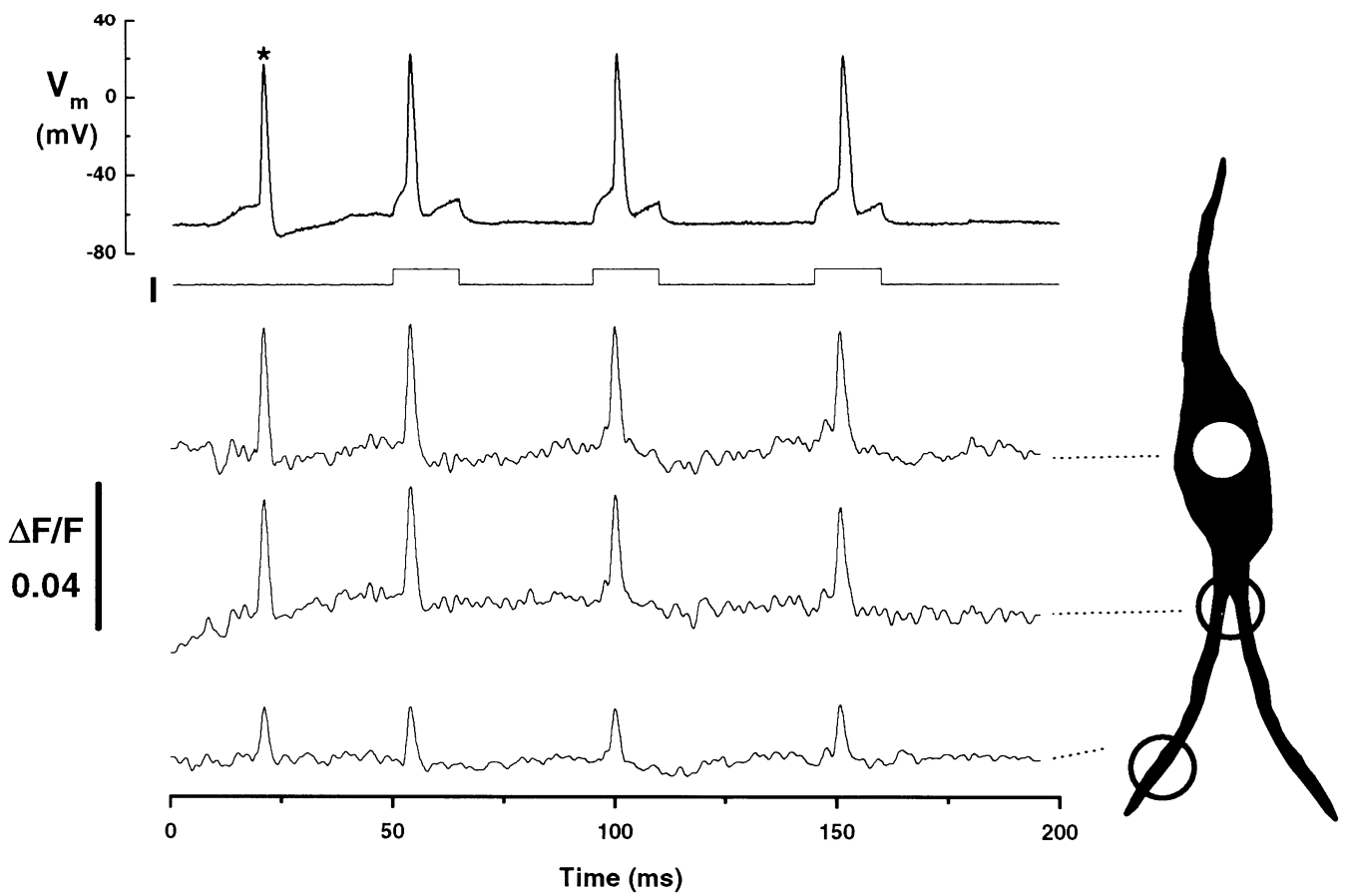

FIGURE 5 Representative membrane potential signals recorded from cultured hippocampal neurons using a voltage-sensitive dye. Spontaneous and evoked action potentials elicited by current injection (100 pA) in cultured hippocampal neurons (7–28 days in culture). These cells had previously been stained (5 min) by bath application of 100 μM di-8-ANEPPS (Molecular Probes) in bath saline. The locations of scanning points are depicted on an outline drawing of the cell (*right*; somatic patch pipette omitted for clarity). A spontaneous action potential is indicated by the asterisk. Optical signals were sampled at 6 kHz (16-bit resolution) and digitally filtered at 1.5 kHz. Scanning spot size = 7 μm. Electrical signals were acquired by whole-cell patch recordings (patch pipette resistance = 4 MΩ) in current-clamp mode by using an Axon Instruments Axopatch 200A amplifier. Electrical signals were prefiltered at 2 kHz and digitized at 7.5 kHz (12-bit resolution). Pipette solution (in mM): K gluconate 120, KCl 20, $MgCl_2$ 1, NaATP 5, NaGTP 0.25, EGTA 10, HEPES 10, pH 7.4. Bath saline (in mM): NaCl 140, $CaCl_2$ 2, KCl 4, $MgCl_2$ 1, HEPES 10, D-glucose 10, pH 7.3.

electrical records obtained via a patch pipette (in current clamp mode) on the soma with the optical records from the same point (Fig. 5). Furthermore, other scanning sites on this proximal dendrite indicate that this type of recording can be made from quite small neuronal structures where signal strength is significantly reduced. These signals could be recorded from small dendritic structures up to 150 μm from the soma. Beyond this point, the dendrites typically became very small and the signal strength quite weak. The optical records presented here demonstrate that small optical signals can be captured that possess a high signal-to-noise ratio and that faithfully represent the equivalent electrical transients.

The ability to capture small membrane potential signals such as postsynaptic potentials is demonstrated in Fig. 6. In this record, excitatory postsynaptic potentials (EPSPs) have been elicited by focal stimulation of presynaptic terminals in the dendritic arborization of a single hippocampal neuron. Focal stimulation was accomplished by local application of hyperosmotic saline through a patch pipette to small distal dendrites (Bekkers and Stevens, 1996). This record captured from two points proximal to the stimulation site demonstrates that small membrane potential signals can be adequately captured from dendritic and somatic structures with a signal-to-noise ratio sufficient to resolve these events without averaging. The size of these signals, as verified by electrical recording at the soma, was between 5 and 15 mV, indicating that they were at least similar in size to unitary EPSP responses. Furthermore, the nature of these signals closely approximated spontaneously occurring EPSPs recorded electrically at the soma (not shown). Moreover, the relative size of the optical signal corresponds closely to similarly recorded action potentials (compare to Fig. 5). Control sweeps in the absence of focal stimulation documented only background noise or occasional spontaneous EPSPs. Closer inspection of these records illustrates that the rate of decay seen in these EPSP waveforms (indicated by *dotted lines*) varies between dendritic and somatic sites. This effect could be due to cable filtering or regional differences in membrane properties and demonstrates the usefulness of obtaining spatially resolved membrane potential signals. The capability to record such signals at the resolution (spatial and temporal) described above represents a significant advance over previous studies (e.g., Chien and Pine, 1991a,b) using similar multisite optical recording methods and voltage-sensitive dyes (but see Salzberg et al., 1977).

The efficacy of this instrument to undertake long-term experiments, especially considering its incorporation of strong laser illumination, is also illustrated in Fig. 6. This figure demonstrates that long-exposure ($\geq$1 s) recordings could be made from the same scanning spot without any obvious photodynamic damage or decline in signal quality. In other experiments, repeated recordings made with intermittent and scanning laser illumination were possible for up to 15 min of recording time or the equivalent of 10 s of continuous illumination before any decline was noted. This

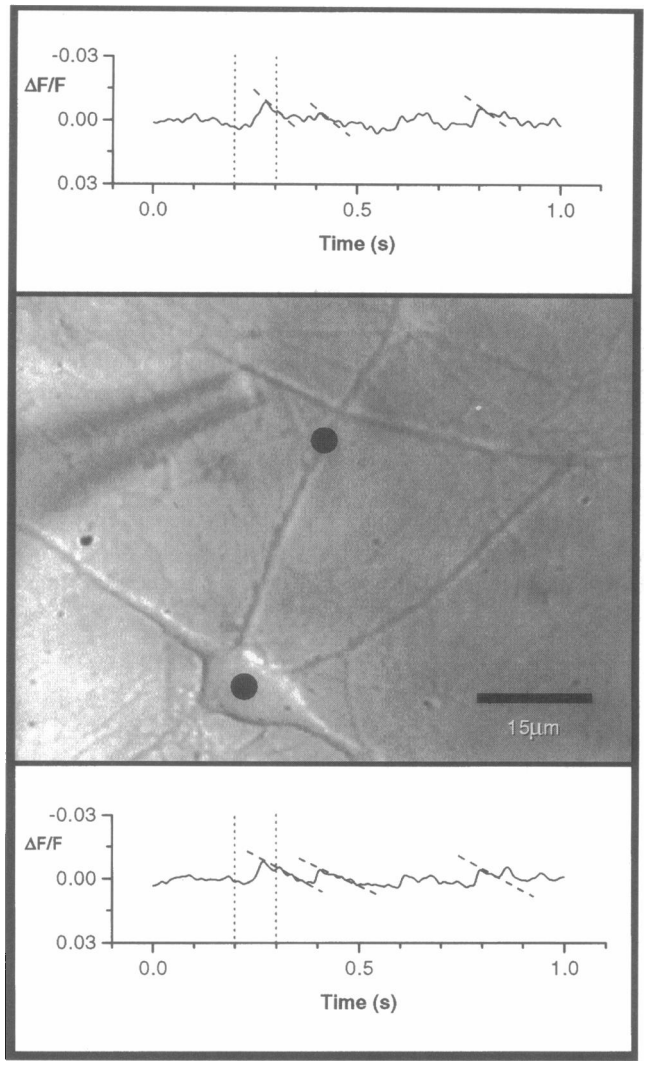

FIGURE 6 Representative postsynaptic potentials recorded from cultured hippocampal neurons using voltage-sensitive dye. Representative EPSPs recorded from dendritic (*top trace*) and somatic (*bottom trace*) recording points after stimulation with hyperosmotic saline (500 mM sucrose in normal saline, *vertical dotted lines*). The location of the scanning spots is indicated by black dots (not to scale). Control recordings taken immediately before and after local application of hyperosmotic saline showed no activity. Signals were sampled at 3 kHz (16-bit resolution) and filtered at 300 Hz. Cells and bath saline as above (except that 100 μM 4-AP was added to the bath saline). Scanning spot size = 2 μm.

value is consistent with the findings of others using this VSD (Rohr and Salzberg, 1994a). In comparison, continuous laser illumination of a cell for even a few seconds typically resulted in severe dye bleaching, a reduction in signal size, and a dramatic decline in cellular input resistance.

Corresponding recordings with the calcium indicator Calcium Orange (Molecular Probes) indicate that optical signals generated by small calcium transients can also be measured. For instance, Fig. 7 demonstrates that stepwise calcium entry can be resolved during a train of action potentials elicited by current injection. Quantifiable steps in

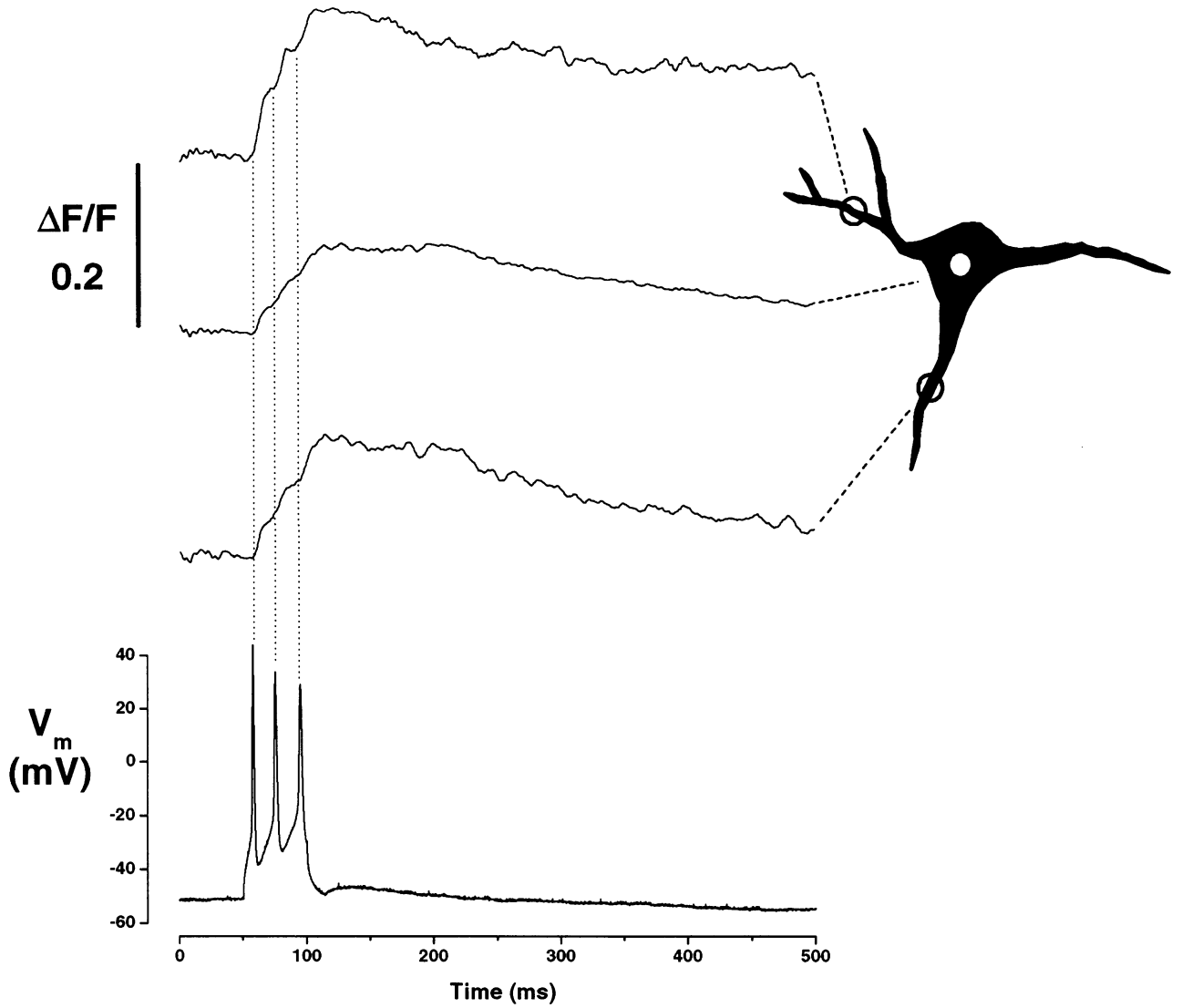

FIGURE 7 Representative calcium transients recorded from cultured hippocampal neurons using Calcium Orange. Calcium Orange-1 N (50 μM; Molecular Probes) was applied through a patch pipette (4 MΩ) on the soma of a cultured hippocampal neuron. The locations of scanning points are depicted on an outline drawing of the cell. Optical signals were sampled at 6 kHz (16-bit resolution) and filtered at 40 Hz. Electrical signals were acquired by whole-cell patch recordings (patch pipette resistance = 4 MΩ) in current-clamp mode by using an Axon Instruments Axopatch 200A amplifier. Electrical signals were prefiltered at 2 kHz and digitized at 7.5 kHz (12-bit resolution). Current injection = 100 pA. Scanning spot size = 7 μm. Pipette solution (in mM): K gluconate 120, KCl 20, $MgCl_2$ 1, NaATP 5, NaGTP 0.25, HEPES 10, pH 7.4. Bath saline was as in Fig. 5.

intracellular calcium can be seen with each successive action potential. The absolute magnitude of calcium entry during such action potentials is probably quite small (Llinas et al., 1981). Furthermore, these records demonstrate a difference in the kinetics of calcium entry between the soma and proximal dendrites. Such differences would probably not be faithfully recorded in slower video rate systems. In fact, recent studies (Etter et al., 1996) using near-membrane indicators have shown that localized calcium transients can be quite fast and that their true kinetics may not be faithfully recorded by using traditional cytoplasmic indicators (e.g., Fura-2).

Together, these records demonstrate that the microscope described here can generate high-resolution, high-fidelity signals from small neuronal structures without any averaging. Furthermore, these records illustrate this instrument's usefulness for making long-term, noninvasive optical recordings.

DISCUSSION

In this report we have presented the design and implementation of a high-speed, random-access, laser-scanning fluorescence microscope developed in our laboratory. This instrument was specifically designed to record fast physiological signals from small neuronal structures and has five main features that distinguish it from other scanning microscopes currently in use. These include a random-access scanning capability, very high temporal resolution, variable spatial

resolution, high digitizing resolution, and multiple noise reduction procedures. Furthermore, this microscope is unique because it incorporates laser illumination in a manner compatible with long-term VSD recordings.

Random-access scanning

An important feature of this system is that each recording point is individually addressed and can be randomly accessed. Furthermore, we have constructed this system to allow the number of scanning points and the rate at which they can be sampled to be independently controlled. Together, these features allow a larger temporal bandwidth and increased flexibility in experiments undertaken with this system. In fact, this approach to fluorescence microscopy may be more correctly termed "scanning photometry," as many points are sampled but no image is formed. In contrast, most scanning microscopes build up an image by raster scanning, whereby each point is visited sequentially for a set period. However, such raster-scanning systems have several disadvantages for physiological studies. Typically, they have no flexibility in the number of points collected, their sampling rate is often fixed, and other signal-to-noise considerations cannot always be optimized. Furthermore, the temporal bandwidth of such systems is severely limited. Only a few systems scan up to video rate (30 frames/s), and even this rate is incompatible with the study of many physiological events, which occur much faster. Moreover, there is no provision for variable integration times or oversampling within many video-rate systems.

To achieve a high-speed, random-access scanning capability, this instrument employs dual acousto-optic deflectors under computer control. In comparison, most scanning microscopes use mechanical methods (e.g., oscillating or rotating mirrors) to scan light (Pawley, 1995). Such mechanical devices are limited by the speed with which they can be moved, by the accuracy with which they can be repeatedly repositioned, and the mechanical noise they produce. In contrast, acousto-optic scanning produces very fast, high-resolution positioning over a large scanning angle without any moving parts. Despite these favorable properties, acousto-optical scanning methods have not been universally accepted. There are several reasons for this. First, it is difficult to achieve both scanning and descanning with the same set of AODs. This has made these devices unattractive for incorporation into confocal microscopes. Several other shortcomings have been proposed (Stelzer, 1995). These include a small deflection angle, limited spatial resolution, a noncircular aperture, low diffraction efficiency, and the chromatic corrections required for different excitation wavelengths or emission light. Again, most of these shortcomings are important only if the AODs are required to descan emission light, as in confocal image formation. For instance, the deflection angle of the AODs used in this study was sufficient to fill the aperture of most objective lenses with only modest intermediate magnification. Furthermore, a spatial resolution of 2 μm was sufficient for the applications proposed here. This value corresponds closely to the size of important neuronal structures, and with smaller spot sizes less tissue would be illuminated and consequently signal strength would be degraded. A noncircular aperture and modest diffraction efficiency were not important considerations in the design of this instrument. Moreover, chromatic corrections required for different laser lines were small and easily made in the software. Finally, AODs have been criticized for producing variations in illumination intensity across the scanning field. This occurs because diffraction efficiency is not always uniform across the acoustic bandwidth of these devices. However, this is only true in some operating modes. For example, the AODs used in this instrument produced uniform scanning spots, provided they were used with laser light that was linearly polarized. In contrast, the AOMs used here exhibited variability in scanning spot intensity. Moreover, because we formed ratios between excitation and emission light as part of our noise correction scheme, any variation in illumination intensity was also compensated for.

This system has been designed with interchangeable deflector combinations that can be optimized for temporal or spatial resolution, depending on the experimental requirements. For instance, in cases where spatial resolution was important, smaller spots (2 μm) were created by using deflectors with higher resolution and larger scan angles, together with smaller system magnification. This spot size roughly corresponded to the size of small dendrites and spines. However, these deflectors exhibit lower acoustic velocity, which increases the aperture time and, therefore, reduces the maximum rate at which the laser beam can be positioned. This relationship is clearly demonstrated by the two deflector combinations used here. The pure AOD produces a better spatial resolution (2 μm) than the AOM (7 μm), but exhibits lower overall bandwidth (200k versus 100k samples/s). These deflector combinations could be readily interchanged because they are contained in identical housings that are mounted in the same way and controlled by the same drivers and software.

The final distinguishing feature of this instrument is the customized user interface that allows considerable flexibility in conducting and interpreting experiments undertaken with this system. This graphical-user interface also includes topographical display capabilities that allow for on-line registration between the physiological signals and the corresponding anatomical structure. Furthermore, all aspects of hardware and software in this system are implemented on a low-cost PC computer.

Together, these features make this scanning configuration unique. While some existing systems do incorporate a single acousto-optic deflector to achieve one dimension of raster scanning (Draaijer and Houpt, 1988), and others have employed dual AODs to perform two-dimensional reflective imaging at video rate (Goldstein et al., 1990, 1993), we have utilized orthogonal acousto-optic deflectors and modulators to achieve very fast two-dimensional scanning for

epifluorescence microscopy. Interestingly, others (Dillon and Morad, 1981; Morad et al., 1986; Miyazaki et al., 1993) have utilized one or two AODs as the basis of a scanning system designed to survey cardiac action potential propagation in the intact heart. However, these systems had relatively modest temporal resolution and lacked any of the useful features present in the current system, such as its random-access scanning capability, variable spatial resolution, high digitizing resolution, and multiple noise reduction procedures.

In summary, we have described one variation of acousto-optic scanning. Specifically, two orthogonal acousto-optic deflectors were used to implement a fast random-access scanning scheme. The primary operational goal of this system was the generation of high temporal resolution. However, this goal was achieved while still maintaining sufficient spatial resolution and scanning area. In many instances, trade-offs were necessary between various operational parameters of these devices, and several experimental criteria were used to empirically derive the best combination of spot size, scanning area, resolution, and scanning rate. Other configurations incorporating acousto-optic devices operating under different conditions are possible. For instance, in situations where larger scan angles or more points are required, different acousto-optic deflectors could be utilized. Furthermore, we have demonstrated that, depending on the experimental objectives, different acousto-optic devices (AOMs and AODs) can be used interchangeably.

Resolution, noise reduction, and signal strength

An important aspect of this system is that optical signals are encoded with high resolution. Both fluorescence and reference signals are digitized with 16-bit resolution. This level of digitizing resolution was essential because the signals from voltage-sensitive dyes are very small (i.e., $\Delta F/F \cong$ 0.1–5%/100 mV). Commercially available scanning microscopes commonly use only 8- or 12-bit detectors or slower oversampling procedures.

The laser-based approach taken here has some fundamental advantages for optimizing the signal-to-noise ratio achievable with VSDs from small neuronal structures. In the ideal case (i.e., shot noise limited measurement) improvements in the signal-to-noise ratio can only be achieved by 1) increased illumination, 2) increased light-gathering efficiency, and 3) decreased system bandwidth (Wu and Cohen, 1993). By incorporating intense laser illumination for very short exposure times, we have maximized peak illumination intensity while minimizing the total illumination seen by the preparation. Thus the likelihood of photodamage and bleaching is reduced, but signal strength is maximized. Despite this advantage, such a scanning approach has one important shortcoming: namely, the temporal bandwidth of the detectors in this type of system must be proportionately greater than an equivalent nonscanning system (e.g., photodiode arrays). An increased temporal bandwidth is typically achieved at the expense of detector sensitivity. Hence the advantage of more intense laser illumination must be balanced against the higher overall system bandwidth required.

An additional feature of this instrument is the on-line signal-processing scheme that is used to correct for variations in fluorescence resulting from fluctuations in the laser light intensity or differences in scanning spot brightness generated by the AODs. This correction scheme uses point-by-point division with a reference signal collected from a second detector, which samples the small amount of excitation light passing through the dichroic mirror. This noise correction scheme is unique, as it has allowed the incorporation of laser sources for high-resolution VSD studies. Alternative methods of noise reduction, such as active beam stabilization (Cohen et al., 1972), have not proved especially successful, because such feedback systems require enormous bandwidth and high loop gain (P. Saggau, unpublished observations). Such systems are inherently unstable. Similarly, subtractive strategies have also proved unsuccessful, principally because of the requirement to exactly match signal sizes.

Detectors

Silicon photodiodes were the detector of choice in this system. These devices were chosen over more sensitive detectors (e.g., photomultiplier tubes (PMTs) or avalanche photodiodes (APDs)) for several reasons. First, these photodiodes possess a high quantum efficiency (i.e., 0.9), particularly at the long wavelengths emitted by VSDs. The equivalent value for PMTs is typically less than 0.1. Because the signal-to-noise ratio in a shot-noise-limited measurement is proportional to the square root of the number of photons collected, a silicon photodiode will perform better than an equivalent device with a lower quantum efficiency, all other things being equal (Cohen and Lesher, 1986). In general, the amount of fluorescence generated by these probes does not require large amplification or very sensitive detectors, especially in cases where the light-gathering capability is close to the theoretical limit. Second, no signal-independent offset could be tolerated, because this severely compromises the ratio formation process between signal and reference detectors, which is needed to remove intrinsic laser fluctuations. Such offsets were present in the output of APDs tested (Bullen and Saggau, unpublished observations). Finally, silicon photodiodes are less expensive and easier to handle than other equivalent detectors.

VSD studies

The performance of this system compares favorably with other systems used to make similar optical recordings with equivalent resolution. Although direct comparison is difficult because of differences in the VSDs employed and even differences in staining properties of the same VSD in different preparations (Ross and Reichardt, 1979; Loew et al.,

1992), it is informative to compare the signal-to-noise ratio achieved in other studies conducted with comparable resolution. For instance, Chien and Pine (1991a,b) employed fluorescent VSDs to study spatially resolved membrane potential signals from cultured rat sympathetic neurons. In this study, full-field epifluorescence illumination and a 256-pixel fiber optic camera were used to collect membrane potential signals with a variety of different VSDs. Direct comparison of the results obtained here with the instrumentation developed by Chien and Pine (1991a,b) shows a significantly larger bandwidth (>5 kHz versus 300 Hz), better spatial resolution (2 μm versus 45 μm), larger signal sizes (10% versus 0.5%), and a better signal-to-noise ratio (20–30 versus <10). Although many of these parameters are dye dependent, it should be noted that these authors screened 24 other dyes, including di-4-ANEPPS (a close relative of di-8-ANEPPS). Other instrumental factors that might have been limiting in the Chien and Pine study included insufficient digitizing resolution (11 bits versus 16 bits) and poor collection efficiency (N.A. = 0.75 versus 1.3). Moreover, the signal quality obtained here also compares favorably with more recent studies using intracellular VSDs (Antic and Zecevic, 1995; Zecevic, 1996). These authors utilized invertebrate neurons from *Helix aspera* and the VSD dye JPW-1114 to investigate spike initiation and conduction in complex neuronal arborizations. They were able to achieve significantly improved signal-to-noise ratio over previous studies employing similar methods (Grinvald et al., 1987). In particular, they were able to distinguish strong regional differences in membrane potential and multiple spike-initiation zones within a single neuron. However, in many cases signal averaging still had to be used, and the signal-to-noise ratio of these recordings was insufficient to record nonstationary postsynaptic potentials. Although direct comparison is difficult, it should also be noted that the neurons studied in these experiments were significantly larger than those used in the current study and thus signal strength was likely greater.

Trade-offs

A number of trade-offs were made in the design and implementation of this methodology. In particular, the need to obtain images and physiological signals simultaneously has been circumvented. Instead, we have chosen to utilize a stationary DIC image to select points for further study under conditions that maximize temporal resolution and provide a higher signal-to-noise ratio from indicators such as VSDs. This trade-off has also allowed us to record with high spatial resolution while maintaining a large temporal bandwidth and optimizing signal-to-noise considerations.

The incorporation of a single detector that collected data in a serial fashion also represents an important trade-off. The bandwidth of such a detector must, by definition, be larger than an equivalent parallel device, and consequently the sensitivity and signal-to-noise ratio achievable would be less. Ideally, a randomly accessed array of photodiodes would provide larger bandwidth, better sensitivity, and a higher signal-to-noise ratio. The cost and sophistication of such a device would be much greater, however.

Future improvements

A number of refinements could further enhance the scope and sophistication of the experiments undertaken with this microscope. For instance, the usefulness of this instrument has recently been increased by the incorporation of an additional detector for experiments employing multiple indicators (Patel et al., 1995) or ratiometric determination using two emission wavelengths (Bullen and Saggau, 1997). Experiments that employ two probes to record different parameters from the same scanning point require indicators with matched excitation and distinct emission spectra. This combination is easily achieved because many VSDs exhibit a large difference between excitation and emission wavelengths (i.e., Strokes shift) and therefore are easily combined with other indicators. Suitable indicators for calcium, sodium, and magnesium are currently available for use with VSDs (Haugland, 1992). Others in our laboratory have recently demonstrated the feasibility of this approach (Sinha et al., 1995). Other applications of the random-access AO scanning principles outlined here could include modified confocal detection schemes for fast optical recording from three-dimensional structures (e.g., brain slices) or high-resolution photolysis of caged compounds.

SUMMARY AND CONCLUSIONS

In summary, we have successfully demonstrated the design and implementation of a high-speed, random-access, laser-scanning fluorescence microscope constructed to record small optical signals from fine neuronal structures with high temporal resolution. Moreover, through the use of laser illumination, high digitizing resolution, and noise reduction techniques (ratio formation, variable sampling times, and variable spot sizes), we have maximized the signal-to-noise ratio achievable from weakly fluorescent structures stained with indicators that give relatively small changes in signal size. Together, these improvements have allowed the development of an instrument that overcomes many of the inherent limitations of classical electrophysiological approaches and will facilitate future investigations into a wide range of neurobiological issues.

We are grateful to Drs. L. B. Cohen, C. M. Colbert, and N. V. Shen for comments on an earlier version of this paper and to B. M. Salzberg for technical guidance in various aspects of this project.

This work was supported in part by grants from the National Science Foundation (BIR-95211685 to AB) and the National Institutes of Health (NS33147 to PS).

REFERENCES

Antic, S., and D. Zecevic. 1995. Optical signals from neurons with internally applied voltage-sensitive dyes. *J. Neurosci.* 15:1392–1405.

Bekkers, J. M., and C. F. Stevens. 1996. Cable properties of cultured hippocampal neurons determined by sucrose-evoked miniature EPSPs. *J. Neurophysiol.* 75:1250–1255.

Bullen, A., and P. Saggau. 1994. Dendritic membrane potential transients from hippocampal neurons in culture measured by high speed laser scanning microscopy. *Soc. Neurosci. Abstr.* 20:891.

Bullen, A., and P. Saggau. 1995. Membrane potential transients in small dendrites from hippocampal neurons measured by high speed laser scanning microscopy. *Soc. Neurosci. Abstr.* 21:597.

Bullen, A., and P. Saggau. 1997. Fast ratiometric measurements of membrane potential using a voltage-sensitive dye and high-speed, random-access laser-scanning microscopy. *Biophys. J* 72:A24.

Chien, C.-B., and J. Pine. 1991a. Voltage-sensitive dye recordings of action potentials and synaptic potentials from sympathetic microcultures. *Biophys. J.* 60:697–711.

Chien, C.-B., and J. Pine. 1991b. An apparatus for recording synaptic potentials from neuronal cultures using voltage-sensitive fluorescent dyes. *J. Neurosci. Methods.* 38:93–105

Cohen, L. B., H.-P. Höpp, J.-Y. Wu, Ch. Xiao, J. London, and D. Zecevic. 1989. Optical measurements of action potential activity in invertebrate ganglia. *Annu. Rev. Physiol.* 51:527–541.

Cohen, L. B., R. D. Keynes, and D. Landowne. 1972. Changes in axon light-scattering that accompany the action potential: current dependent components. *J. Physiol. (Lond.).* 244:727–52.

Cohen, L. B., and S. Lesher. 1986. Optical monitoring of membrane potential: methods of multisite optical measurement. *In* Optical Methods in Cell Physiology. P. DeWeer and B. M. Salzberg, editors. Wiley-Interscience, New York. 71–99.

Cohen, L. B., and B. M. Salzberg. 1978. Optical methods for monitoring neuron activity. *Annu. Rev. Neurosci.* 1:171–182.

Cummings, D., S. Rohr, A. L. Obaid, and B. M. Salzberg. 1992. Multiple site optical recording of synchronized bursts in neocortical and hippocampal cell cultures using voltage-sensitive dyes. *Soc. Neurosci. Abstr.* 18:1057.

Dillon, S., and M. Morad. 1981. A new laser scanning system for measuring action potential propagation in the heart. *Science.* 214:453–456.

Draaijer, A., and P. M. Houpt. 1988. A standard video-rate confocal laser-scanning reflected and fluorescence microscope. *Scanning.* 10: 139–145.

Ebner, T. J., and G. Chen. 1995. Use of voltage-sensitive dyes and optical recordings in the central nervous system. *Prog. Neurobiol.* 46:463–506.

Etter, E. F., A. Minta, M. Poenie, and F. S. Fay. 1996. Near-membrane [Ca^{2+}] transients resolved using the Ca^{2+} indicator FFP18. *Proc. Natl. Acad. Sci. USA.* 93:5368–5373.

Goldstein, S. R., T. Hubin, S. Rosenthal, and C. Washburn. 1990. A confocal video-rate scanning reflected-light microscope with no moving parts. *J. Microsc.* 157:29–38.

Goldstein, S. R., T. Hubin, and T. G. Smith. 1993. An improved no-moving-parts video-rate confocal microscope. *Micron Microsc. Acta.* 23:437–446.

Grinvald, A. 1985. Real-time optical mapping of neural activity: from single growth cones to the intact mammalian brain. *Annu. Rev. Neurosci.* 8:263–305.

Grinvald, A., and I. C. Farber. 1981. Optical recording of calcium action potentials from growth cones of cultured neurons with a laser microbeam. *Science.* 212:1164–1167.

Grinvald, A., B. M. Salzberg, V. Lev-Ram, and R. Hildesheim. 1987. Optical recording of synaptic potentials from processes of single neurons using intracellular potentiometric dyes. *Biophys. J.* 51:643–651.

Haugland, R. P. 1992. Handbook of Fluorescent Probes and Research Chemicals. Molecular Probes, Eugene, OR.

Lieke, E. E., R. D. Frostig, A. Arieli, D. Y. Tso, R. Hildesheim, and A. Grinvald. 1989. Optical imaging of cortical activity: real-time imaging using extrinsic dye signals and high resolution imaging based on slow intrinsic signals. *Annu. Rev. Physiol.* 51:543–559.

Llinas, R., I. Z. Steinberg, and K. Walton. 1981. Presynaptic calcium currents in squid giant synapse. *Biophys. J.* 33:289–322.

Loew, L. M. 1993. Potentiometric membrane dyes. *In* Fluorescent and Luminescent Probes for Biological Activity. W. T. Matson, editor. Academic Press, London. 150–160.

Loew, L. M., L. B. Cohen, J. Dix, E. N. Fluhler, V. Montana, G. Salama, and W. Jian-Young. 1992. A naphthyl analog of the aminostyryl pyridinium class of potentiometric membrane dyes shows consistent sensitivity in a variety of tissue, cell and model membrane preparations. *J. Membr. Biol.* 130:1–10.

Milton, G., C. L. M. Ireland, and J. M. Ley. 1983. Electro-optic and acousto-optic scanning and deflection. *In* Optical Engineering, Vol. 3. Marcel Dekker, New York and Basel.

Miyazaki, Y., Y. Ishiguro, and T. Sato. 1993. Optical probing of active membrane potential using lasers and microoptics. *Jpn. J. Physiol.* 43(Suppl. 1):S53–S56.

Morad, M., S. Dillion, and J. Weiss. 1986. An acousto-optically steered laser scanning system for measurement of action potential spread in intact heart. *In* Optical Methods in Cell Physiology. P. DeWeer and B. M. Salzberg, editors. Wiley-Interscience, New York. 211–226.

Patel, S. S., A. Bullen, and P. Saggau. 1995. Simultaneous multi-site recording with two fluorescent probes using high-speed laser random scanning microscopy. *Soc. Neurosci. Abstr.* 21:1078.

Pawley, J. B. 1995. Handbook of Biological Confocal Microscopy. Plenum, New York.

Rohr, S., and B. M. Salzberg. 1994a. Multiple site optical recording of transmembrane voltage (MSORTV) in patterned growth heart cell cultures: assessing electrical behavior, with microsecond resolution, on a cellular and subcellular scale. *Biophys. J.* 67:1301–1315.

Rohr, S., and B. M. Salzberg. 1994b. Characterization of impulse propagation at the microscopic level across geometrically defined expansions of excitable tissues: multiple site optical recording of transmembrane voltage (MSORTV) in pattern growth heart cell cultures. *J. Gen. Physiol.* 104:287–309.

Ross, W. N., and L. F. Reichardt. 1979. Species-specific effects on the optical signals of voltage-sensitive dyes. *J. Membr. Biol.* 48:343–356.

Saggau, P. 1994. Optical recording from neural populations in vitro: applications of laser scanning microscopy. *In* Enabling Technologies for Cultured Neural Networks. D. A. Stenger and T. M. McKenna, editors. Academic Press, San Diego. 187–205.

Saggau, P., R. Hiendl, and F. Rucker. 1990. Simultaneous multisite monitoring of neural activity by laser scanning microscopy. *Soc. Neurosci. Abstr.* 16:1097.

Salzberg, B. M. 1983. Optical recording of electrical activity in neurons using molecular probes. *In* Current Methods in Cellular Neurobiology, Vol. III, Electrophysiological and Optical Recording Techniques. J. L. Barker and J. F. McKelvy, editors. Wiley, New York. 139–188.

Salzberg, B. M. 1989. Optical recording of voltage changes in nerve terminals and fine neuronal processes. *Annu. Rev. Physiol.* 51:543–559.

Salzberg, B. M., A. Grinvald, L. B. Cohen, H. V. Davila, and W. N. Ross. 1977. Optical recording of neuronal activity in an invertebrate central nervous system. Simultaneous monitoring of several neurons. *J. Neurophysiol.* 40:1281–1291.

Sinha, S. R., S. S. Patel, and P. Saggau. 1995. Simultaneous optical recording of evoked and spontaneous transients of membrane potential and intracellular calcium concentration with high spatio-temporal resolution. *J. Neurosci. Methods.* 60:49–60.

Stelzer, E. H. K. 1995. The intermediate optical system of laser-scanning confocal microscopes. *In* Handbook of Biological Confocal Microscopy. J. B. Pawley, editor. Plenum, New York. 139–154.

Sutor, B., J. J. Hablitz, F. Rucker, and G. TenBruggencate. 1994. Spread of epileptiform activity in the immature rat neocortex studied with voltage-sensitive dyes and laser scanning microscopy. *J. Neurophysiol.* 72: 1756–1768.

Wilson, T., and C. Sheppard. 1984. Theory and Practice of Optical Scanning Microscopy. Academic Press, London.

Wu, J.-Y., and L. B. Cohen. 1993. Fast multisite optical measurement of membrane potential. *In* Fluorescent and Luminescent Probes for Biological Activity. W. T. Matson, editor. Academic Press, London. 389–404.

Xu, J., and R. Stroud. 1992. Acousto-Optic Devices: Principles, Design and Applications. Wiley, New York.

Zecevic, D. 1996. Multiple spike-initiation zones in single neurons revealed by voltage-sensitive dyes. *Nature.* 381:322–325.